Journal of Materials Chemistry A

Accepted Manuscript

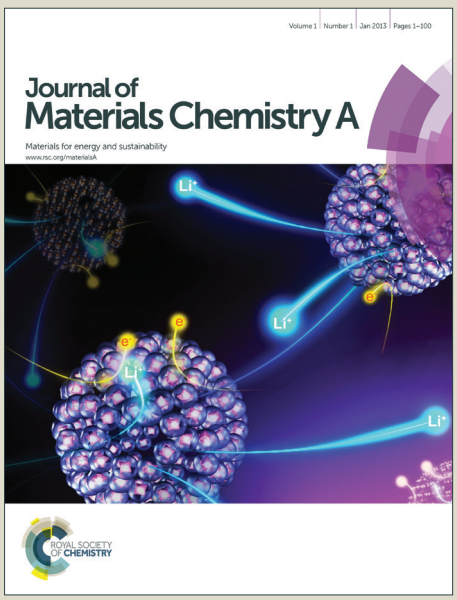

ROYAL SOCIETY OF CHEMISTRY

www.rsc.org/materialsA

Centrifugation-free and high yield synthesis of nanosized H-ZSM-5 and its structure-guided aromatization of methanol to 1, 2, 4-trimethylbenzene

Kui Shen[ab], Weizhong Qian[a]*, Ning Wang[a], Chang Su[a], and Fei Wei[a]

[a]Beijing Key Laboratory of Green Chemical Reaction Engineering and Technology, Department of Chemical Engineering, Tsinghua University, Beijing 100084, P.R. China;

[b]School of Chemistry and Chemical Engineering, South China University of Technology, Guangzhou 510640, P.R.China.

ABSTRACT: Nanosized H-ZSM-5 has been proven an efficient way to improve mass transport property with shape selectivity in many catalytic reactions. Generally, the synthesis of very fine nanosized H-ZSM-5 always suffers from low product yield and complicated centrifugal separation process, which severely hinder its large-scale preparation and industrial applications. Herein, we report a centrifugation-free and high yield synthesis route for hierarchically nanosized ZSM-5 with a wide Si/Al ratio range by a combination of pre-aging process and steam-assisted conversion method using alkalis-free powder as the ZSM-5 precursor. This facile route not only avoids the energy-intensive centrifugal separation and ion-exchange process, but also greatly increases the crystallization efficiency with high yield. The obtained nanosized ZSM-5 possesses ultrafine uniform size, high surface area, high total pore volumes, tunable Si/Al molar ratio and high crystallinity. As a result, the nanosized ZSM-5 shows excellent catalytic performance when used in the catalytic conversion of methanol to aromatics. Notably, the nanosized ZSM-5 with a Si/Al_{th} of 60 (NZS-60) shows almost 25-fold longer catalytic lifetime as well as up to 16% higher total aromatic selectivity when compared with conventional ZSM-5. Furthermore, the selectivity of 1, 2, 4-trimethylbenzene over this catalysts can be up to 44% in all products and 64% in aromatics products. Characterization results of the spent samples reveal that the most-improved catalytic performance and high selectivity of 1, 2, 4-trimethylbenzene over the nanosized ZSM-5 could be attributed to its small crystal size and hierarchical structure, which not only prevented the deposition of polyaromatic hydrocarbon in the microspores, but also sharply increased the reaction efficiency of bulky intermediate products in the surface of catalyst.

KEYWORDS: *Methanol; Nanosized; ZSM-5; Zeolites; MTA reaction; Coke deposition.*

1. INTRODUCTION

The limited availability of crude oil stimulates the study of new processes using other cheap or renewable resources to prepare aromatics,[1-7] which is one of the most important raw materials for chemical industry and is basically produced by petrochemical processes such as reforming and cracking using crude oil.[5, 8, 9] Among these alternative processes, catalytic conversion of methanol to aromatics (MTA) is a promising technology for the production of aromatics with high quality, and thus has attracted extensive attention.[10-12] ZSM-5 zeolite with MFI structure has been proved to be a highly effective catalyst for the aromatization of a wide range of feedstocks, because of its well-defined channels, high surface area, tunable acidity and high hydrothermal stability.[2, 5, 7, 13-15] The ZSM-5 zeolite has unique molecular-sized micropores with sinusoidal channels of 0.55 nm x 0.51 nm in [100], and straight channels of 0.56 nm x 0.53 nm in [010], and thus shows excellent shape selectivity in many aromatization reactions.[2, 5, 7, 16, 17] However, these definite micropores could cause severe diffusion resistance of larger molecules in the zeolite and thus often result in quick deactivation by the deposition of carbonaceous residues that block the reactants from accessing the active sites.[13, 14, 18-20] Nanosized ZSM-5 zeolite has short channel in all a,b,c-axis directions and allows the quick diffusion of reactant or intermediate products and, consequently, exhibited much longer life time in high temperature catalytic processes, compared to conventional microsized ZSM-5. However, the annual amount of nanosized ZSM-5 produced to this date is far lower than that of microsized ZSM-5, owing to the following apparent engineering challenges. First, traditional synthesis routes for nanosized ZSM-5, mainly concentrating on the confined space synthesis[21-26] and clear solutions synthesis,[27-30] is normally conducted in aqueous solutions with NaOH as the mineralizer.[21, 22] So, the as-prepared nanosized Na-ZSM-5 in crystallization liquid always require repeated energy-intensive centrifugal separation and ion-exchange process to obtain the final active H-form nanosized ZSM-5. The great energy consumption and long time operation seriously retard its commercial application. Second, hydrothermal synthesis of nanosized ZSM-5

always suffers from low product yield and thus results in stringent environmental regulations by the uncrystallized aluminosilicate and serious loss of the centrifugal separation in remaining synthesis solution.[27, 29, 31, 32] It is, therefore, highly desirable to develop a novel route for nanosized H-ZSM-5 in terms of simplicity, reproducibility and large-scale applicability for MTA process.

Herein, we report a centrifugation-free and high yield route for nanosized H-ZSM-5 with excellent structural properties by a combination of pre-aging process and steam-assisted conversion (SAC) method using alkalis-free powder as the ZSM-5 precursor. The thorough characterization and systematic study of synthesis conditions indicate that the nanosized ZSM-5 with ultrafine size (30-60 nm), wide Si/Al ratio range, high surface area (above 440 m^2/g), high total pore volumes (above 0.7 cm^3/g), and high crystallinity can be obtained by a two-step approach with an aging time of 72 h in 90 ^oC and an NH_4NO_3/SiO_2 molar ratio of 0.017-0.34. Then, these obtained nanosized ZSM-5 catalysts with different densities of acid sites (Si/Al_{th}=30, 60 and 90) are applied as a solid acid catalyst for the catalytic conversion of methanol to aromatics. The reaction results indicate the nanosized ZSM-5 has much better catalytic stability and higher selectivity of 1, 2, 4-trimethylbenzene compared to conventional ZSM-5. To determine why, we study thoroughly the deactivated catalysts and monitor the quantity and location of coke formation during the reaction.

2. EXPERIMENTAL SECTION

2.1. Centrifugation-free and high yield synthesis of nano-sized ZSM-5

The reactants used in the synthesis are tetraethylorthosilicate (TEOS, Beijing Modern Eastern Fine Chemicals Co., Ltd), tetrapropylammonium hydroxide (TPAOH, 25% in water, Zhejiang Ken Te Chemical Co., Ltd.), Aluminium nitrate nonahydrate ($Al(NO_3)_3.9H_2O$, Beijing Chemical Works) and ammonium nitrate (NH_4NO_3, Beijing Chemical Works).

In this study, three samples with Si/Al_{th} molar ratio of 30, 60 and 90 (denoted as NZS-30, NZS-60 and NZS-90) are synthesized using this facile synthesis route to certify the tunable Si/Al of our route to cater the strict operation condition of MTA reaction. In a typical synthesis of nanosized ZSM-5, 24.3 g TEOS, used as silica

source, is added into 25.8 g TPAOH with continuous stirring. The molar composition of the gel is 92 SiO_2: 25 TPAOH: 479 H_2O: 368 EtOH. The presence of ethanol (EtOH) in the mixed gel is due to the hydrolysis of TEOS with H_2O. After homogenizing at room temperature for 1 h, the mixture is hydrothermally treated at 90 ^oC for 72 h. After cooling down, the solution containing a little water, 0.58-1.43 g $Al(NO_3)_3.9H_2O$, and 0-0.75 g NH_4NO_3 is added to the mixture slowly. The resulting mixture is further stirred for about 1 h, and then heated at 60 ^oC to complete dryness. The resulting dry precursor lumps are coarsely crushed. Then, 5 g precursor powder is transferred into a 15 mL Teflon cup, which itself is placed into a 70 mL Teflon liner with a support. 2 g of distilled water is poured at the bottom of the liner without contacting the dry gel in the inner Teflon cup. The charged liner assembly is placed into an 80 mL steel reactor and transferred into a preheated oven at the 180^oC and heated for 24 h. The crystallization reaction is subsequently quenched by cold water. The obtained powder is directly dried at 110 ^oC overnight without centrifugal separation and ion-exchange steps, and subsequently calcined in air at 550 ^oC for 5 h to remove the template (TPAOH) to obtain the final H-form nanosized ZSM-5.

For comparison purposes, three conventional Na-ZSM-5 with the Si/Al_{th} of 30, 60, and 90 (Fig. S2) are also synthesized according to the method reported by JC Groen et al[33] with a little modification. The corresponding H-ZSM-5 (denoted as CZS-30, CZS-60 and CZS-90, respectively) is prepared through ion-exchange three times and calcination with conventional Na-ZSM-5 as the starting material. Detailedly, the obtained conventional Na-ZSM-5 is firstly converted to the ammonium form by cation-exchange in a NH_4NO_3 solution. Five grams of Na-ZSM-5 is dispersed in 100 ml NH_4NO_3 solution (1M) and vigorously stirred for 6 h. The solid products were collected by filtering separation. The exchange process is performed repeatedly 3 times to complete the exchange reaction, and NH_4-ZSM-5 is formed. The final C-ZSM-5 product is obtained by calcining the NH_4-ZSM-5 powder at 550 ^oC for 5 h. In order to investigate the necessity of cation-exchange process, the N-ZSM-5 obtained directly by direct synthesis route is also ion-exchanged according to the process above except using centrifugal separation with a high speed of 12000 r /min

for 30 min.

2.2. Characterization of the fresh ZSM-5 samples

X-ray diffractions (XRD) are recorded with a Rigaku D/Max-RB diffractometer using Cu Kα Radiation at 40 kV and 120 mA. Scanning electron microscope (SEM) images are performed by a high-resolution scanning electron microscope (JEOL, JSM-7401) at 3.0 kV. TEM experiments are performed on a high-resolution transmission electron microscope (JEOL, JEM-2010, exited at 120kV). Brunauer–Emmett–Teller (BET) surface area are recorded in a Quantachrome automated surface area and porosity analyzer with N_2 as the adsorption gas. NH_3-TPD is recorded in a Quantachrome automated chemisorption analyzer from room temperature to 850℃ with a ramp of 10℃/min. The Si/Al of the zeolite is obtained by inductively coupled plasma optical emission spectrometer (ICP-OES, IRIS Intrepid II XSP). NMR spectra are obtained on a Varian Infinityplus-400 spectrometer. Brønsted acid sites and Lewis acid sites were determined by pyridine adsorption. The samples are first dried, in situ, by heating to 723 K under vacuum, and then were cooled to 323 K. At this temperature, the samples are exposed to pyridine vapour using an equilibration time of 30 min. After physically adsorbed pyridine molecules being removed by outgassing at 423 K for 1 h, IR spectra are collected at 423 K with 4 cm^{-1} resolution using a Nicolet FTIR spectrometer.

2.3. Catalytic conversion of methanol to aromatics

Before catalytic test, all the samples are modified with 2 wt% Zn by traditional incipient wetness impregnation using aqueous solutions of Zn $(NO_3)_2$. $6H_2O$. Then the Zn-modified samples are dried overnight, and calcinated in air at 823 K for 5 h.

The MTA reactions are performed at the conditions of 1 atm, 748 K and WHSV =0.75 h^{-1} (under N_2 flow (10 mL min^{-1})) in a conventional fixed bed stainless steel reactor (13.0 mm i.d) equipped with a thermocouple in the middle of the catalyst bed. 0.70 g of catalyst is placed in the fixed bed reactor. The flow rate of pure methanol and N_2 is controlled using a dual micro-plunger pump and the mass flow controllers,

respectively. The products (hydrocarbons) are analyzed using two flame ionization detector (FID). The conversion of methanol and the selectivity of different products were calculated (carbon base) by considering oxygenates (methanol and dimethylether) as the unconverted reactant.

2.4. Analysis of partially deactivated catalysts

The partially deactivated catalysts after catalytic tests are characterized by TGA-DSC, nitrogen adsorption, TEM and GC-MS to investigate the factors resulting in the superior catalytic performance of the nanosized ZSM-5. TGA-DSC is performed using a thermo gravimetric analyzer (TGA/DSC-1) in the range 30-900 ℃ at a heating rate of 10 ℃ min^{-1} in air. The coke species formed on the deactivated catalysts after reactions are also characterized by gas chromatography-mass spectroscopy (GC-MS). The coke species are extracted by the following method developed by Guisnet[34] with a little modification. To obtain the relative concentrations of the organics formed over different samples, the exactly same amount (20 mg) of the deactivated catalyst is always dissolved in 1 mL of 15% HF solution. Organic species are then extracted with 0.8 mL $C(CH_3)_2Cl_2$ and analyzed using GC-MS (MSD 5973, EI 70 eV) with a HP-5MS column (30 m, 0.25 mm i.d.), and the graphite carbon in the water phase is characterized by TEM experiments.

Further, the location and the amount of coke in Zn/NZS-60 are analyzed as a function of the reaction time using the previously reported methods.[35-37] The total amount of coke (external+internal) within the partially deactivated Zn/NZS-60 at different reaction time is obtained using TGA analysis. The amount of the internal coke is estimated from the decrease in micropore volume (determined by N_2 adsorption measurements) relative to the pristine sample, by assuming a coke density of 1.22 g/cm^3. The external coke is calculated by subtracting the internal coke content from the total coke content.

3. RESULTS AND DISCUSSION

3.1. Characterization of the fresh ZSM-5 samples.

The preparation of N-ZSM-5 is also shown schematically in Fig. 1. The steam

assisted conversion (SAC) method is a very efficient method for preparing zeolites. [38-41] In our route using SAC method, very little water necessary for crystallization is always kept separate from precursor powder during the crystallization reactions. Obviously, after the crystallization process, the products are in solid phase, free of alkali ions, which could be directly converted to the H-form nanosized ZSM-5 for acid catalytic applications only via calcination. In addition, the avoidance of solvents in the synthesis and repeated wash process for removing NaOH not only significantly reduces the waste production, but also greatly enhances its crystallization efficiency with high yield.

Fig. 2 shows the representative low and high magnification SEM images of the nanosized ZSM-5 prepared by our route. The SEM images clearly show that the N-ZSM-5 is composed of many spherical crystallites with uniform sizes of about 50 nm. To further confirm the particle sizes and the structure, the nanosized ZSM-5 are studied by transmission electron microscopy (TEM). The TEM images (Fig. 3a-c) reveal abundant mesoporous network through the assembly of these uniform nanosized ZSM-5 crystals. Analysis with HR-TEM images in Fig. 3d-f elucidates that all the samples are completely crystalline, as the parallel lattice fringes can be clearly observed and spread throughout the entire crystals. Individual particles can be recognized with average sizes of about 50 nm. Obviously, the Si/Al of the ZSM-5 precursor hardly affects the size and morphology of the final products, which is different from the general pattern when using hydrothermal methods.[42] The absence of sponge-like material in the SEM and TEM pictures indicates the absence of amorphous material. Since no silica and aluminium source are washed away in the whole synthetic route, the yield of these nanosized ZSM-5 is nearly 100%, in stark contrast to the low yields of nanoparticles usually obtained from conventional hydrothermal route.[27, 29, 42, 43]

The stacking of these nanosized crystals produces the substantial mesoporosity, leading to different pore structure from the conventional ZSM-5 (Fig. S2). Nitrogen adsorption/desorption isotherms and BJH pore size distribution are shown in Fig. 4. The CZS-30 shows a typical type-I isotherm corresponding to the solely microporous

structure. However, all isotherms of the nanosized H-ZSM-5 exhibit a typical adsorption curve of type I plus type IV with an apparent enhanced uptake and an obvious hysteresis loop in the P/Po range of 0.8 to1, indicating its remarkable micro-/mesoporous structure.[24, 44, 45] Correspondingly, pore size analysis by the BJH method using the adsorption branch of the isotherm (Fig. 4b) shows that all the nanosized H-ZSM-5 possess a broad pore distribution with a mean pore size of about 20 nm. As a result, the nanosized H-ZSM-5 have a much higher BET area and a larger mesopore volume than the CZS-30. As summarized in Table 1, the BET surface area increases from 388 m^2g^{-1} for the CZS-30 up to 441.5-484.0 m^2 g^{-1} for nanosized ZSM-5. The total pore volume increases from 0.19 cm^3 g^{-1} to 0.72-0.76 cm^3 g^{-1} and mesopore volume increases from 0.04 cm^3 g^{-1} to more than 0.58-0.62 cm^3 g^{-1}. It is also worth noting that the textural properties do not noticeably change while increasing the Si/Al of the nanosized H-ZSM-5.

The XRD patterns of all samples (Fig. 5a) show five well-resolved peaks at 7.98 °, 8.82 °, 23.18 °, 24.02 ° and 24.46°, which are in good agreement with high crystalline MFI-structured ZSM-5 without any impurities or amorphous phase.[30, 46] The XRD line widths of all the nanosized H-ZSM-5 are much broader than those for CZS-30 due to their smaller crystal size.[47] Fig. 5b shows the UV Raman spectra of the samples excited at 325 nm. All samples show the characteristic bands of the MFI structure with a wide band at 380 cm^{-1} (Fig. 5b), which is associated with the framework symmetric stretching vibration of a five-membered building unit in ZSM-5 zeolites.[32, 48, 49] Generally，the catalytically active acid sites of ZSM-5 are always correlated to the presence of intra-framework aluminum atoms. Thus, successful incorporation of aluminum atoms into the silica framework of nanosized ZSM-5 with wide Si/Al_{th} is verified by ^{27}Al MAS NMR spectroscopy. As shown in Fig. 5c, the ^{27}Al MAS-NMR spectra of all the samples show only one sharp aluminum peak at 52 ppm indicating that all the aluminum atoms is incorporated into the ZSM-5 framework with tetrahedral coordination environment.[50] In addition, the ^{29}Si MAS NMR spectra of all samples (Fig. S3) show similar features with a sharp peak at −112 ppm and a small peak at −105 ppm. The sharp peak can be attributable to Si(0Al)

contribution and the small peak to the Si(1Al) contribution,[51] which further confirm the present of framework aluminum in the nanosized ZSM-5. Thus, the nanosized ZSM-5 with a wide range of Si/Al can be prepared directly by this facile direct synthesis route.

Furthermore, the different textural properties brought about by crystal sizes might induce remarkable changes of surface properties, which play a crucial role in the catalytic performance of zeolite-based catalysts. The infrared spectra of the dehydrated of CZS-30 (Fig. 5d) show no obvious peaks because of the broad background peak. In sharp contrast, the infrared spectra of three nanosized ZSM-5 in the region of OH stretching vibrations show a major band at 3745 cm^{-1} attributed to silanol groups, which is in agreement with its decreased crystal sizes and increased external surface area. It is reported that this type of Si-related defective sites is very effectual to increase yields of aromatics and paraffins for MTH reaction.[52] Besides, additional spectral components of lower intensity are found over nanosized ZSM-5 , which could be attributed to: 1) perturbed silanols mainly located inside the zeolite crystals (3727 cm^{-1}), 2) Al(OH)Si groups corresponding to strongly acidic Brønsted sites (3612 cm^{-1}), and 3) a broad band corresponding to silanols interacting through hydrogen bonding (3500 cm^{-1}). As for NZS-60 and NZS-90, the intensity of the bands at 3745 cm^{-1} and 3500 cm^{-1} are more strong than NZS-30, suggesting that the Si/Al of nanosized ZSM-5 could influence its surface characteristic significantly. There are hardly any peaks at about 3660 cm^{-1} ascribed to OH groups bound to extra-framework and/or perturbed framework Al atoms,[52, 53] indicating successful incorporation of all aluminum atoms into the silica framework of the samples.

In order to certify the feasibility of our synthesis route, we compare the acidic properties of pristine nanosized ZSM-5 and the samples after 3 times of ion-exchange. As shown in Fig. 6, minor differences are observed in both the TPD curves (Fig. 6a) and pyridine-absorbed FTIR spectra (Fig. 6b) between the three couples of nanosized ZSM-5, indicating energy-intensive centrifugal separation and ion-exchange process are indeed unnecessary in our route. In addition, Fig. 6a shows that the acid strength is declined sharply with the increase of Si/Al for the nanosized H-ZSM-5, and the

acidity of NZS-30 is also comparable with CZS-30 because of their similar Si/Al_{ICP} (Table 1). It is also noteworthy that the amount of L acid reduces rapidly with the increasing of Si/Al of the nanosized H-ZSM-5 (Fig. 6b). Meantime, the intensity of hydrogen-bonded PyH^+ peak over nanosized ZSM-5 is much strong than CZS-30 due to the enhanced adsorption capacity caused by its large mesopore volume.[54]

3.2. Evolution of the nanosized ZSM-5 with crystallization time

To study the crystallization mechanism of NZS-60, a kinetic run is carried out by varying the synthesis time from 0 h to 24 h at 180 ℃. Fig. 7b shows the XRD patterns of the samples at different reaction times. Before stream-assisted crystallization, the sample exhibits an extremely faint XRD pattern of MFI structure. With the steam-assisted conversion at 180 ℃, the intensity of the characteristic MFI-structured peaks increases rapidly and draws the maximum as the crystallization proceeds up to 3 h, which indicates the amorphous structure of the starting powder could translate into a pure ZSM-5 phase just within 3 h (Fig. 7a). Obviously, the presence of seeds plays an important role in shortening the nucleation stage, which is the most time consuming step in the crystallization of ZSM-5.[49] Interestingly, further increasing crystallization time leads to the slight reduction of crystallinity possibly due to the destructive effect of the template on the framework of the product. It is well reported that TPAOH template plays the role of scaffold forming a meso-structure during the crystallization process.[55] This is confirmed by the N_2 adsorption isotherm and the corresponding pore size distribution. As shown in Fig. 7c, the isotherm of the sample with 0 h crystallization has a near linear uptake over the P/P_o range from 0 to 0.4, which is corresponding to micropores or small mesopores below 3 nm. Upon increasing crystallization time from 0 h to 180 min, uptakes of the isotherms move toward high P/P_o. Correspondingly, the average pore size increases from less than 3 nm in the starting dry gel to about 11 nm in the sample at 180 min crystallization time. Longer crystallization treatment has little effect on the mesoporous structure, since no obvious changes from pore size distribution curves could be observed. Table 2 summarizes the textural properties and crystallinity of the samples at various crystallization times. The external surface area decreases with crystallization time, but

remains very high even after reaching the 100% crystallization. However, both of the total pore volume and the mesopore volume increase within 120 min crystallization time, and finally achieve stability, indicating the high efficiency of our route for obtaining meso/micropore zeolite.

3.3. Effects of gel composition and aging condition

In our preliminary experiments, we discover that the crystal size of the products is sensitive to the concentrations of NH_4^+. Therefore, at an aging temperature of 90°C for 72 h and a constant Si/Al_{th} of 60, the influence of NH_4^+/SiO_2 is investigated and the SEM images of products prepared with different NH_4NO_3/SiO_2 are shown in Fig. 8. When there is no NH_4NO_3 added into the synthesis mixture, the size distribution of the product is broad and most of the ZSM-5 crystal is greater than 100 nm. Products with a uniform diameter of about 50 nm could be obtained within a NH_4/SiO_2 ratio of 0.017-0.034 (Fig. 8b-c). This can be explained by the fact that aluminum incorporation is achieved more easily when the smaller NH_4^+ are available as charge compensators, compared with when only the larger TPA^+ are present. Further increasing the NH_4^+ to 0.067, a sample with a diameter of about 300 nm and a smaller BET surface area is obtained. The increased particle size and the reduced crystallinity of ZSM-5 crystals obtained in this run are probably due to the excessively decreased alkalinity caused by the hydrolysis of plentiful NH_4^+.

In addition, our synthesis route includes the ‘‘pre-aging process’’ before stream-assisted crystallization, which is considered to produces abundant ZSM-5 nuclei (Fig. S1),[56] leading to the formation of small ZSM-5. So, the effect of the pre-aging time on the crystal size of the product is also investigated with other conditions unchanged. Fig. 9 shows the SEM images of the products synthesized with the pre-aging temperature of 90 °C for different time, which indicates that the crystal size is decreased with the increase of pre-aging time. The average crystal sizes of the products at pre-aging times of 0, 24, and 72 h are found to be about 160 nm, 100 nm and 50 nm, respectively. Further extension of the aging time after 72 h has little effect on the crystalline phases and crystal size, since no obvious changes from the SEM

image could be observed.

3.4. Catalytic performances of the nanosized ZSM-5 with different Si/Al.

The methanol to aromatics reaction (MTA) is an important process for the non-oil route to aromatics.[10-12, 57] It is respected that the meso/macroporous structure and the short diffusion length of nanosized ZSM-5 are favorable for the MTA reaction with high stability. Therefore the catalytic performances over 2%Zn-modified nanosized (denoted as Zn/NZS-30, Zn/NZS-60 and Zn/NZS-90) and 2%Zn-modified conventional ZSM-5 (denoted as Zn/CZS-30, Zn/CZS-60 and Zn/CZS-90) in MTA reaction are compared in a fixed bed stainless. Fig. 10 shows an overview of the activities and stabilities of three groups between nanosized and conventional ZSM-5 described in this contribution. It is worth noting that the comparison of catalysts performance is performed under the same Si/Al_{th} ratios because the catalytic properties are more likely to change by Al content. Under so strict operation condition, all catalysts show almost the similar high initial methanol conversions of above 95%. However, as reaction proceeds, the activities of Zn/CZS-30, Zn/CZS-60 and Zn/CZS-90 are all declined gradually just within a few hours. In sharp contrast, all the nanosized ZSM-5 show much superior catalytic stability and higher total aromatics selectivity than the corresponding conventional Zn/ZSM-5 with a same Si/Al_{th}. It is noted that Si/Al_{th} ratios also have a remarkably effect on the catalytic performance of nanosied Zn/ZSM-5 catalysts. Among these catalysts, the Zn/NZS-60 with Si/Al_{th}=60 gives the slowest deactivation with a stable total aromatics selectivity and long catalytic lifetime (defined as the time at which the catalytic conversion decreases by 50%, which is denoted as $t_{1/2}$) of more than 75 h, which is almost 25-fold than that of Zn/CZS-60 ($t_{1/2}$≈3 h). In addition, detailed initial product selectivity is also given in Table S2 and Table S3. Notably, the most stable Zn/NZS-60 shows the high total aromatics selectivity of 68 % with an absolute selectivity of 16 % higher than the CZS-60 (52 %). More importantly, the selectivity of 1, 2, 4-trimethylbenzene over this catalysts can be up to 44 % in all products and 64 % in aromatics products. Compared with previously reported results in the process of MTA,[13, 63, 64] the high selectivity of 1,

2, 4-trimethylbenzene over nanosized Zn/ZSM-5 could decrease intensively the cost and energy consumption of the subsequent separation and purification process to obtain high purity 1, 2, 4-trimethylbenzene. Since the acid strength, acid amount, Si/Al_{ICP} ratio and micropore volume are similar for Zn/NZS-60 and Zn/CZS-60 (Fig. 6, Table 1), the superior catalytic stability and higher 1, 2, 4-trimethylbenzene selectivity over the former can be directly attributed to the unique mesoporous structure and short diffusion length of the nanosized ZSM-5. It is well documented that catalyst deactivation of ZSM-5 is mainly caused by the coke formation on the micropore mouths and in the micropores, which is produced via secondary reactions.[37, 58] So, the micropore blockage would occur very slowly over the nanosized ZSM-5 because of its unique mesoporous structure and the abundant pore mouths at the surface of the nanosized ZSM-5, which not only favour the coke precursor diffusion, but also sharply increase the evacuation of aromatics and make the isomerization reaction of trimethylbenzene to be dynamically balanced, leading to the high selectivity of 1, 2, 4-trimethylbenzene that is the most thermodynamically stable product when the isomerization reaction of trimethylbenzene has reach the thermodynamic equilibrium. Due to the enlarged external surface area and short diffusion path lengths, it is feasible the thermodynamically stable 1, 2, 4-trimethylbenzene formed inside the micropores could readily migrated to the external surface. In the case of solely microporous Zn/CZS-60, the diffusion of this bulk product from the micropores to the external surface would be relatively slow, leading to lower aromatics selectivity and shorter lifetime in MTA process.

In order to verify this point, we conduct a series of characterization over the spent Zn/NZS-60 and Zn/CZS-60, including TG/DSC, GC-MS and TEM. The TG/DTA profiles are shown in Fig. 11. It is obvious that the total weight loss over the spent Zn/NZS-60 is obviously much higher than that over conventional ZSM-5, indicating its much higher capacity of holding coke. However, as the reaction time of Zn/NZS-60 is much longer than the corresponding Zn/CZS-60, the spent Zn/NZS-60 has a slow coke formation rate of 3.78 $mg.g_{cat}^{-1}.h^{-1}$, much lower than that of 26.33 $mg.g_{cat}^{-1}.h^{-1}$ for spent Zn/CZS-60. As shown in Fig. 11b, the DTA profiles of the spent

Zn/CZS-60 has a broad exothermic peak, implying that the coke in this catalyst is composed by various carbon species deposited on active sites. However, there is almost only one sharp exothermic peak around 480 ^{o}C for NZS-60, indicating that the carbon species formed over this catalyst is mainly relatively single coke species, which is also being confirmed by the GC-MS analysis of the retained organic species in spent catalysts by 15% HF dissolution and extraction. As shown in Fig. 12a-b, only a tiny amount of liberating heavy hydrocarbons could be found in the extract phase of Zn/NZS-60, and the main phase of deposits over this sample are graphite carbon, which could not be extracted by CH_2Cl_2 (Fig. 12a). However, significant amounts of polyaromatic hydrocarbon are found over conventional ZSM-5, which could occlude the pore channel and lead to the quick deactivation of the catalysts (Fig. 12b).

Further, in order to understand how the particle size of ZSM-5 is related to the catalytic performance. The location and the amount of coke in Zn/NZS-60 are analyzed as a function of the reaction time using the characterization method described in Section 2.4. As the results in Fig. 12c shown, the coke in Zn/NZS-60 is preferentially deposited at the stacking pores of nanosized ZSM-5 prior to the generation inside the straight and sinusoidal channels with a much slower coking rate than Zn/CZS-60. The coke in the stacking pores is not completely blocked and the reactants and products could still move to the active sites and escape from the micropores. The TEM images and corresponding EDX analysis of the graphite carbon stay in are also verify the above results. As shown in Fig. 12d-e, the graphite carbon, depositing on the outer surface of Zn/NZS-60, forms hollow carbon nanosphere after the inner Zn/NZS-60 being dissolved by 15% HF solution. However, 89% of the coke is formed inside the micropore for the Zn/CZS-60 with solely microporous, which is the main cause of the sudden drop in catalytic activity. Therefore, we, for the first time, validate directly that the coke over nanosized ZSM-5 is preferentially deposited at the outside surface prior to the intracrystalline micropores. Above all, compared with conventional ZSM-5, the nanosized ZSM-5 has the following obvious advantages when used in MTA reaction: (1) having short diffusion length, which could enhances the diffusibility of reactant and product, and prevents the deposition

of polyaromatic hydrocarbon in the microspores; (2) the substantial mesoporosity endows the nanosized ZSM-5 much higher capacity of holding coke than conventional one; (3) high external surface sharply increased the reaction efficiency of bulky intermediate products in the surface of catalyst, leading to high selectivity of 1, 2, 4-trimethylbenzene; (4) abundant surface groups (e.g. silanol groups, perturbed silanols and Al(OH)Si groups) could provide more active site for MTA reaction.

4. CONCLUSIONS

The present work reports a centrifugation-free synthesis route for hierarchical nanosized ZSM-5 with 100% yield by steam-assisted conversion using a solid alkalis-free powder as the ZSM-5 precursor. The obtained nanosized ZSM-5 possesses excellent properties such as ultrafine uniform size, robust thermal stability, high surface area, high total pore volumes, tunable Si/Al molar ratio, and high crystallinity and shows excellent catalytic performance when used in the catalytic conversion of methanol to aromatics. The Zn/NZS-60 shows almost 25 folds catalyst lifetime and up to 16% higher total aromatics selectivity compared with conventional microsized Zn/CZS-60. More importantly, the selectivity of 1, 2, 4-trimethylbenzene over this catalysts can be up to 44 % in all products and 64 % in aromatics products. Analysis of partially deactivated catalysts reveal that the the superior catalytic stability and higher 1, 2, 4-trimethylbenzene selectivity over the nanosized Zn/ZSM-5 could be directly attributed to its small crystal size and mesoporous structure, which prevent the deposition of polyaromatic hydrocarbon in the micropores, but also sharply increase the reaction efficiency of the bulky molecule. The nanosized ZSM-5 prepared by this route shows great potential for large scale industrial applications for MTA process with high selectivity of 1, 2, 4-trimethylbenzene.

■ AUTHOR INFORMATION

Corresponding Author

* E-mail: qianwz@tsinghua.edu.cn (W. Qian).

Notes

The authors declare no competing financial interest.

■ ACKNOWLEDGMENTS

This work was supported by the National 973 program of 2011CB932602 and NSFC key program of 51236004.

■ REFERENCES

[1] T.R. Carlson, Y.T. Cheng, J. Jae and G.W. Huber, *Energy Environ. Sci.*, 2011, **4**, 145.
[2] B. Valle, A.G. Gayubo, A.T. Aguayo, M. Olazar and J. Bilbao, *Energy & Fuels*, 2010, **24**, 2060.
[3] T.R. Carlson, J. Jae, Y.-C. Lin, G.A. Tompsett and G.W. Huber, *J. Catal.*, 2010, **270** 110.
[4] X. Guo, G. Fang, G. Li, H. Ma, H. Fan, L. Yu, C. Ma, X. Wu, D. Deng and M. Wei, *Science*, 2014, **344,** 616.
[5] L. Yu, S. Huang, S. Zhang, Z. Liu, W. Xin, S. Xie and L. Xu, *ACS Catal.*, 2012, **2,** 1203.
[6] Y.T. Cheng and G.W. Huber, *ACS Catal.*, 2011, **1,** 611.
[7] Y.T. Cheng, Z. Wang, C.J. Gilbert, W. Fan and G.W. Huber, *Angew. Chem., Int. Ed.*, 2012, **51,** 11097.
[8] T.F. Degnan Jr, *Top. Catal.*, 2000, **13,** 349.
[9] C. Marcilly, *J. Catal.*, 2003, **216,** 47.
[10] K. Shen, W. Qian, N. Wang, J. Zhang and F. Wei, *J. Mater. Chem. A*, 2013, **1** 3272.
[11] R. Barthos, T. Bánsági, T. Süli Zakar and F. Solymosi, *J. Catal.*, 2007, **247,** 368.
[12] Y. Ni, A. Sun, X. Wu, G. Hai, J. Hu, T. Li and G. Li, *Microporous Mesoporous Mater.*, 2011, **143**, 435.
[13] C.S. Cundy and P.A. Cox, *Chem. Rev.*, 2003, **103**, 663.
[14] A. Corma, *Chem. Rev.*, 1997, **97,** 2373.
[15] F. Pan, X. Lu, Y. Wang, S. Chen, T. Wang and Y. Yan, *Microporous Mesoporous Mater.*, 2014, **184,** 134.
[16] D. Van Vu, M. Miyamoto, N. Nishiyama, Y. Egashira and K. Ueyama, *J. Catal.*, 2006, **243** 389.
[17] M.B. Roeffaers, R. Ameloot, M. Baruah, H. Uji-i, M. Bulut, G. De Cremer, U. Müller, P.A. Jacobs, J. Hofkens and B.F. Sels, *J. Am. Chem. Soc.*, 2008, **130,** 5763.
[18] V. Valtchev, E. Balanzat, V. Mavrodinova, I. Diaz, J. El Fallah and J.-M. Goupil, *J. Am. Chem. Soc.*, 2011, **133,** 18950.
[19] H. Jin, M.B. Ansari and S.-E. Park, *Chem. Commun.*, 2011, **47,** 7482.
[20] S.I. Cho, S.D. Choi, J.H. Kim and G.J. Kim, *Adv. Funct. Mater.*, 2004, **14,** 49.
[21] C.H. Jacobsen, *Chem. Commun.* (1999) 673.
[22] I. Schmidt, C. Madsen and C.J. Jacobsen, *Inorg. Chem.*, 2000, **39,** 2279.

[23] P.-S. Lee, X. Zhang, J.A. Stoeger, A. Malek, W. Fan, S. Kumar, W.C. Yoo, S. Al Hashimi, R.L. Penn and A. Stein, *J. Am. Chem. Soc.*, 2010, **133,** 493.
[24] H. Chen, J. Wydra, X. Zhang, P.-S. Lee, Z. Wang, W. Fan and M. Tsapatsis, *J. Am. Chem. Soc.*, 2011, **133,** 12390.
[25] W.C. Yoo, S. Kumar, R.L. Penn, M. Tsapatsis and A. Stein, *J. Am. Chem. Soc.*, 2009, **131,** 12377.
[26] W. Fan, M.A. Snyder, S. Kumar, P.-S. Lee, W.C. Yoo, A.V. McCormick, R.L. Penn, A. Stein and M. Tsapatsis, *Nature mater.*, 2008, **7,** 984.
[27] R. Van Grieken, J. Sotelo, J. Menendez and J. Melero, *Microporous Mesoporous Mater.*, 2000, **39,** 135.
[28] S. Lee, C.S. Carr and D.F. Shantz, *Langmuir*, 2005, **21,** 12031.
[29] W. Song, V. Grassian and S. Larsen, *Chem. Commun.*, 2005, 2951.
[30] Y.-Q. Deng, S.-F. Yin and C.-T. Au, *Ind. Eng. Chem. Res.*, 2012, **51**, 9492.
[31] J. Aguado, D. Serrano and J. Rodriguez, *Microporous Mesoporous Mater.*, 2004, **75**, 41.
[32] L. Ren, Q. Wu, C. Yang, L. Zhu, C. Li, P. Zhang, H. Zhang, X. Meng and F.-S. Xiao, *J. Am. Chem. Soc.*, 2012, **134**, 15173.
[33] J.C. Groen, T. Bach, U. Ziese, A.M. Paulaime-van Donk, K.P. de Jong, J.A. Moulijn and J. Pérez-Ramírez, *J. Am. Chem. Soc.*, 2005, **127,** 10792.
[34] M. Guisnet and P. Magnoux, *Appl. Catal.*, 1989, **54,** 1.
[35] D. Bibby, N. Milestone, J. Patterson and L. Aldridge, *J. Catal.*, 1986, **97,** 493.
[36] F.L. Bleken, K. Barbera, F. Bonino, U. Olsbye, K.P. Lillerud, S. Bordiga, P. Beato, T.V. Janssens and S. Svelle, *J. Catal.*, 2013, **307,** 62.
[37] M. Choi, K. Na, J. Kim, Y. Sakamoto, O. Terasaki and R. Ryoo, *Nature*, 2009, **461**, 246.
[38] S.P. Naik, A.S. Chiang and R. Thompson, *J. Phys. Chem. B*, 2003, **107**, 7006.
[39] J. Yao, H. Wang, S.P. Ringer, K.-Y. Chan, L. Zhang and N. Xu, *Microporous Mesoporous Mater.*, 2005, **85**, 267.
[40] K. Zhu, J. Sun, J. Liu, L. Wang, H. Wan, J. Hu, Y. Wang, C.H. Peden and Z. Nie, *ACS Catal.*, 2011, **1**, 682.
[41] N. Ren, B. Subotić, J. Bronić, Y. Tang, M. Dutour Sikirić, T. Mišić, V. Svetličić, S. Bosnar and T. Antonić Jelić, *Chem. Mater.*, 2012, **24**, 1726.
[42] V.B. Mortola, A.P. Ferreira, J.M. Fedeyko, C. Downing, J.M. Bueno, M.C. Kung and H.H. Kung, *J. Mater. Chem.*, 2010, **20**, 7517.
[43] S.C. Larsen, *J. Phys. Chem. C* , 2007, **111**, 18464.
[44] X. Liu, B. Tian, C. Yu, F. Gao, S. Xie, B. Tu, R. Che, L.M. Peng and D. Zhao, *Angew. Chem., Int. Ed.*, 2002, **41**, 3876.
[45] M. Imperor-Clerc, P. Davidson and A. Davidson, *J. Am. Chem. Soc.*, 2000, **122**, 11925.
[46] F. Liu, T. Willhammar, L. Wang, L. Zhu, Q. Sun, X. Meng, W. Carrillo-Cabrera, X. Zou and F.-S. Xiao, *J. Am. Chem. Soc.*, 2012, **134**, 4557.
[47] J. Kim, M. Choi and R. Ryoo, *J. Catal.*, 2010, **269**, 219.
[48] Y. Yu, G. Xiong, C. Li and F.-S. Xiao, *J. Catal.*, 2000, **194**, 487.

[49] K. Shen, W. Qian, N. Wang, C. Su and F. Wei, *J. Am. Chem. Soc.*, 2013, **135**, 15322.
[50] T.-O. Do, A. Nossov, M.-A. Springuel-Huet, C. Schneider, J.L. Bretherton, C.A. Fyfe and S. Kaliaguine, *J. Am. Chem. Soc.*, 2004, **126**, 14324.
[51] C. Fyfe, G. Gobbi, G. Kennedy, J. Graham, R. Ozubko, W. Murphy, A. Bothner-By, J. Dadok and A. Chesnick, *Zeolites*, 1985, **5**, 179.
[52] P. Sazama, B. Wichterlova, J. Dedecek, Z. Tvaruzkova, Z. Musilova, L. Palumbo, S. Sklenak and O. Gonsiorova, *Microporous Mesoporous Mater.*, 2011, **143**, 87.
[53] S. Zheng, H.R. Heydenrych, A. Jentys and J.A. Lercher, *J. Phys. Chem. B*, 2002, **106**, 9552.
[54] W. Song, R. Justice, C. Jones, V. Grassian and S. Larsen, *Langmuir*, 2004, **20**, 8301.
[55] J. Wang, J.C. Groen, W. Yue, W. Zhou and M.-O. Coppens, *Chem. Commun.*, 2007, 4653.
[56] H. Mochizuki, T. Yokoi, H. Imai, R. Watanabe, S. Namba, J.N. Kondo and T. Tatsumi, *Microporous Mesoporous Mater.*, 2011, **145**, 165.
[57] M. Conte, J.A. Lopez-Sanchez, Q. He, D.J. Morgan, Y. Ryabenkova, J.K. Bartley, A.F. Carley, S.H. Taylor, C.J. Kiely and K. Khalid, *Environ. Sci. Technol.*, 2012, **2,** 105.
[58] L. Narasimhan, J. Thybaut, G. Marin, J. Denayer, G. Baron, J. Martens and P. Jacobs, *Chem. Eng. Sci.*, 2004, **59**, 4765.

Table 1. Textural properties and compositions of various samples.

Sample name	Si/Al_{th} atomic ratio[a] (mol mol^{-1})	Si/Al_{ICP} atomic ratio[b] (mol mol^{-1})	BET surface area (m^2g^{-1})	Mesopore surface area[c] ($cm^3 g^{-1}$)	Total pore volume ($cm^3 g^{-1}$)	Micropore Volume[c] ($cm^3 g^{-1}$)	Mesopore Volume[d] ($cm^3 g^{-1}$)
CZS-30	30	24.1	388.2	33.1	0.19	0.15	0.04
NZS-30	30	28.6	484.0	118.6	0.73	0.15	0.58
NZS-60	60	56.2	441.5	100.4	0.72	0.14	0.58
NZS-90	90	84.4	446.7	107.7	0.76	0.14	0.62

[a] *The theoretical Si/Al based on the molar composition of the initial gel.*

[b] *Measured by ICP-OES.*

[c] *t-plot method.*

[d] $V_{meso}=V_{tot}-V_{micro.}$

Table 2. Textural properties and crystallinity of the NZS-60 crystallized at various time.

crystallization time (min)	Crystallinity[a] (%)	BET surface area (m^2g^{-1})	Mesopore surface area[c] ($cm^3\ g^{-1}$)	Total pore volume ($cm^3\ g^{-1}$)	Micropore Volume[c] ($cm^3\ g^{-1}$)	Mesopore Volume[d] ($cm^3\ g^{-1}$)
0	0.04	1081.5	-	0.58	-	-
40	19.37	854.0	547.4	0.84	0.14	0.70
70	54.46	593.9	189.3	0.88	0.16	0.72
120	75.57	519.9	137.0	0.93	0.17	0.76
180	100.00	472.8	119.4	0.86	0.15	0.71
240	99.87	466.4	115.6	0.77	0.15	0.62
1440	95.10	441.5	100.4	0.72	0.14	0.58

[a] *calculated via XRD result by assuming the maximum crystallinity of the product after 180 min of crystallization time is 100% .*

[b] *t-plot method.*

[d] $V_{meso}=V_{tot}-V_{micro.}$

[c] *t-plot is not applicable because of the continuous distribution of pore sizes around 3 nm.*

Table 3. Methanol conversion and product selectivity of MTA reactions over various catalysts used in the present study measured after the reactions being stable.

Catalysts[a]	Conversion of methanol (%)	Selectivity, (%)						Total aromatics (%)
		C_1-C_5 alkanes	C_2-C_5 olefins	C_6 ben.	C_7 ben.	C_8 ben.	C_{9+} ben.	
Zn/CZS-30	99.03	20.83	28.95	1.76	11.19	36.09	1.16	50.22
Zn/CZS-60	96.80	16.77	31.23	0.64	5.29	34.57	11.49	51.99
Zn/CZS-90	95.54	16.02	27.43	0.81	7.19	31.88	16.65	56.54
Zn/NZS-30	99.47	15.06	22.80	0.48	3.71	25.88	32.07	62.15
Zn/NZS-60	99.37	24.36	7.69	0.32	2.07	14.60	50.95	67.94
Zn/NZS-90	99.41	18.12	11.32	0.50	3.20	14.62	52.21	70.55

[a] *The sampling time (Zn/CZS-30, Zn/CZS-60, Zn/CZS-90 : 1.2 h, Zn/NZS-6: 3.6 h, and Zn/NZS-90: 10.2)*

Table 4. The distribution of trimethylbenzene selectivity over various catalysts used in the present study measured measured after the reactions being stable.

Catalysts[a]	Selectivity in products, (%)			Selectivity in aromatics, (%)		
	1,3,5 tri-ben	1,2,4 tri-ben	1,2,3 tri-ben	1,3,5 tri-ben	1,2,4 tri-ben	1,2,3 tri-ben
Zn/CZS-30	-	1.16	-	-	2.31	-
Zn/CZS-60	-	10.92	-	-	21.00	-
Zn/CZS-90	0.53	15.52	0.58	0.94	27.45	1.03
Zn/NZS-30	2.38	27.66	2.02	3.83	44.51	3.25
Zn/NZS-60	3.90	44.12	2.92	5.74	64.94	4.30
Zn/NZS-90	4.53	44.40	3.57	6.42	62.93	5.06

[a] *The sampling time (Zn/CZS-30, Zn/CZS-60, Zn/CZS-90 : 1.2 h, Zn/NZS-6: 3.6 h, and Zn/NZS-90: 10.2)*

List of Fig.s Captions

Fig. 1. Schematic diagram of centrifugation-free synthetic procedures for the nanosized ZSM-5 with tunable Si/Al molar ratio.

Fig. 2. SEM images of (a) NZS-30, (b) NZS-60 and (c)NZS-90, and high-magnification SEM images of (d) NZS-30 , (e) NZS-60 and (f) NZS-90, which are taken from the part surrounded with a white frame in (a), (b) and (c).

Fig. 3. Low-magnification TEM images of (a) NZS-30, (b) NZS-60 and (c)NZS-90, and high-magnification TEM images of (d) NZS-30 , (e) NZS-60 and (f) NZS-90, which was taken from the part surrounded with a white frame in (a), (b) and (c).

Fig. 4. (a) Nitrogen adsorption/desorption isotherms and (b) BJH pore size distribution curves calculated from the adsorption branch of the isotherm (inset) for NZS-30, NZS-60, NZS-90 and CZS-30.

Fig. 5. (a) XRD patterns, (b) UV-Raman spectra and (c) ^{27}Al-NMR spectra of the NZS-30, NZS-60, NZS-90 and CZS-30. (d) FT-IR spectra of the dehydrated NZS-30, NZS-60, NZS-90 and CZS-30.

Fig. 6. (a) NH_3-TPD adsorption spectra of the NZS-30, NZS-60, NZS-90 and CZS-30. (b) FTIR spectra of the dehydrated NZS-30, NZS-60, NZS-90 and CZS-30

Fig. 7. Investigation on the crystallization process of NZS-60. (a) SEM image of the product crystallized at 180 ^{o}C for 180 min, (b) XRD patterns, (c) Nitrogen adsorption/desorption isotherms, and (d) BJH pore size distribution calculated from the adsorption branch of the isotherm for the samples crystallized at various crystallization time.

Fig. 8. SEM images of the NZS-60 prepared with an NH_4NO_3/SiO_2 molar ratio of (a) 0, (b) 0.017, (c) 0.034, and (d) 0.067, indicating that a trace amount of NH4NO3 addition to precursor gel markedly reduce the particle sizes of the NZS-60.

Fig. 9. SEM images of the NZS-60 prepared with an aging time of (a) 0 h, (b) 36 h, (c) 72 h, and (d) 144h, indicating that the particle size of NZS-60 is decreased

with an increase in the pre-aging time.

Fig. 10. Methanol conversions and overall aromatics selectivity with various Zn/ZSM-5 samples as a function of time-on-stream

Fig. 11. (a) TG and (b) DSC profiles of the spent Zn/CZS-60 and Zn/NZS-60. Oxidation gas :20%O_2/N_2, heating rate 10 $^oC\ min^{-1}$.

Fig. 12. (a) Photographs of the spent catalysts after being dissolved in 15% HF and extracted by CCl4. (b) GC-MS chromatograms of the organic species in spent catalysts extracted by CH2Cl2. (c) Coke formation over Zn/NZS-60 with various time-on-stream during MTA reaction. (d) and (e) TEM images of the graphite carbon depositing on the outer surface of Zn/NZS-60 after the inner Zn/NZS-60 being dissolved by 15% HF solution. (f) The corresponding EDX spectrum of the graphite carbon.

Figures

Fig. 1. Schematic diagram of centrifugation-free synthetic procedures for the nanosized ZSM-5 with tunable Si/Al molar ratio.

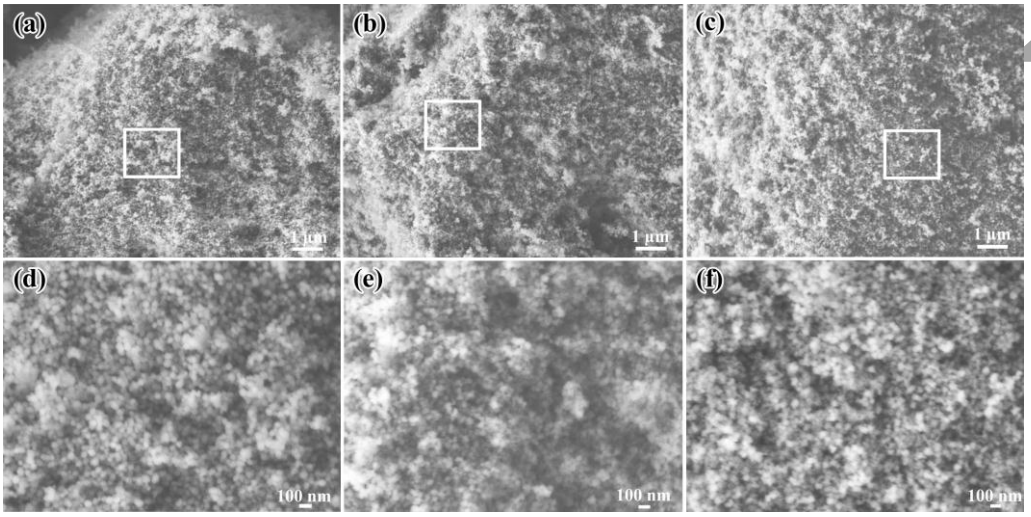

Fig. 2. SEM images of (a) NZS-30, (b) NZS-60 and (c)NZS-90, and high-magnification SEM images of (d) NZS-30 , (e) NZS-60 and (f) NZS-90, which are taken from the part surrounded with a white frame in (a), (b) and (c).

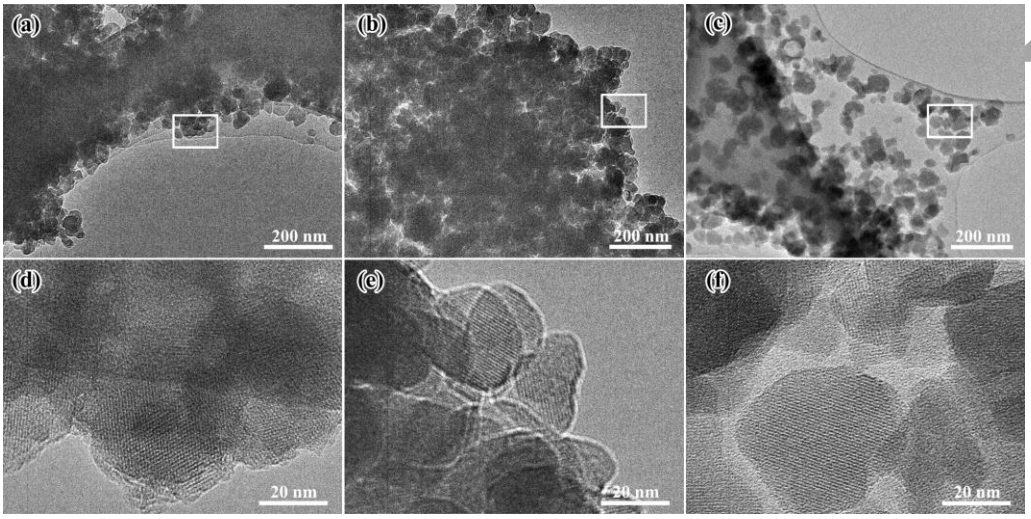

Fig. 3. Low-magnification TEM images of (a) NZS-30, (b) NZS-60 and (c)NZS-90, and high-magnification TEM images of (d) NZS-30 , (e) NZS-60 and (f) NZS-90, which was taken from the part surrounded with a white frame in (a), (b) and (c).

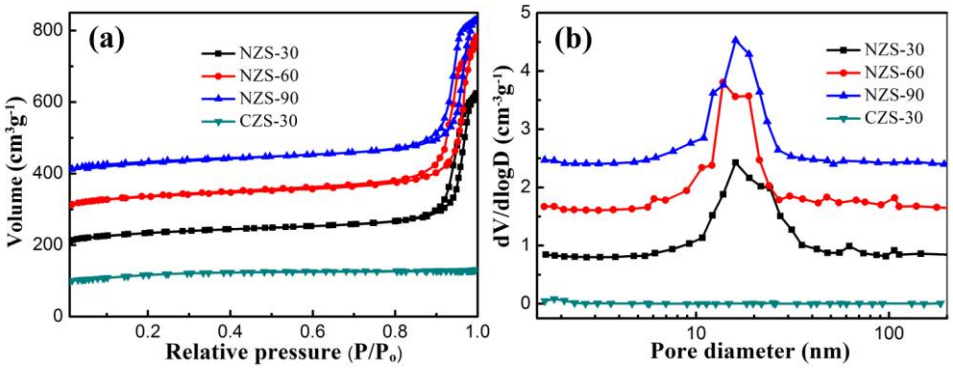

Fig. 4. (a) Nitrogen adsorption/desorption isotherms and (b) BJH pore size distribution curves calculated from the adsorption branch of the isotherm (inset) for NZS-30, NZS-60, NZS-90 and CZS-30. The isotherms are offset vertically by 100, 200 and 300 cm^3g^{-1} and the pore size distribution curves are offset vertically by 0.8, 1.6 and 2.4 $cm^3\ g^{-1}$ for NZS-30, NZS-60 and NZS-90, respectively.

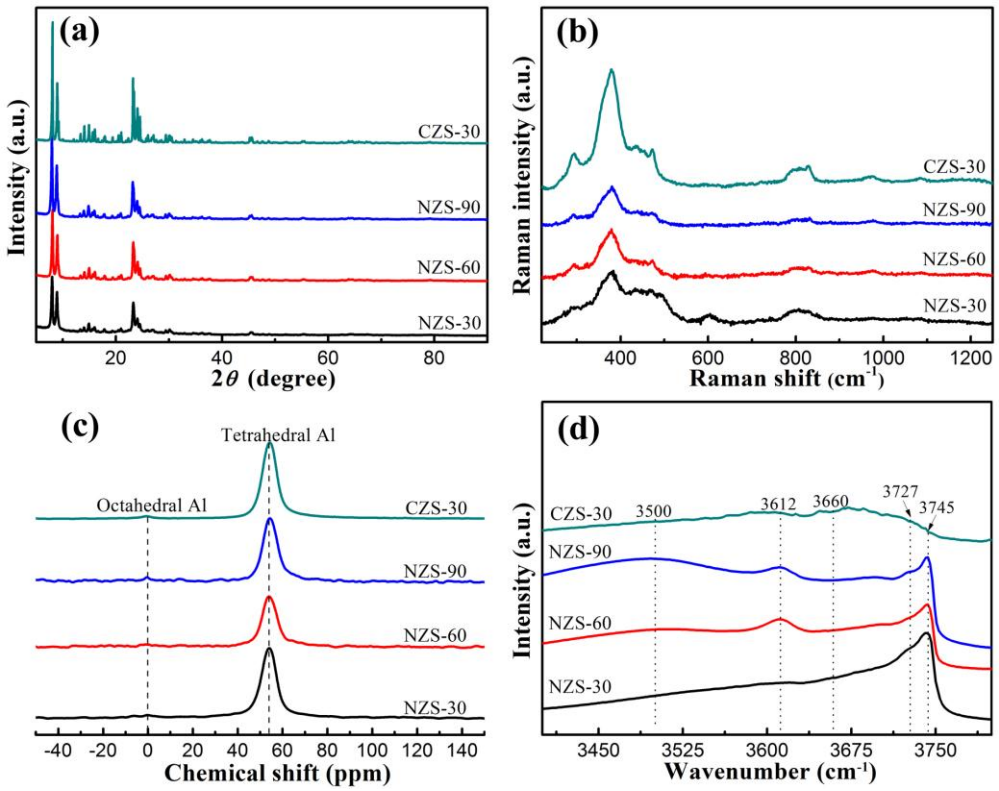

Fig. 5. (a) XRD patterns, (b) UV-Raman spectra and (c) ^{27}Al-NMR spectra of the NZS-30, NZS-60, NZS-90 and CZS-30. (d) FT-IR spectra of the dehydrated NZS-30, NZS-60, NZS-90 and CZS-30.

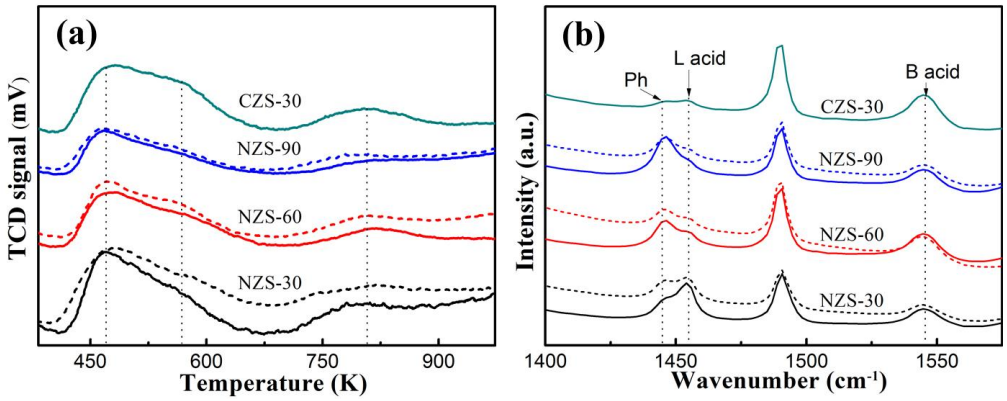

Fig. 6. (a) NH_3-TPD adsorption spectra of the NZS-30, NZS-60, NZS-90 and CZS-30. (b) FTIR spectra of the dehydrated NZS-30, NZS-60, NZS-90 and CZS-30 after desorbing of pyridine at 323 K and then desorbing at 423 K under high vacuum (the dotted curve are the corresponding samples after 3 times ion-exchange).

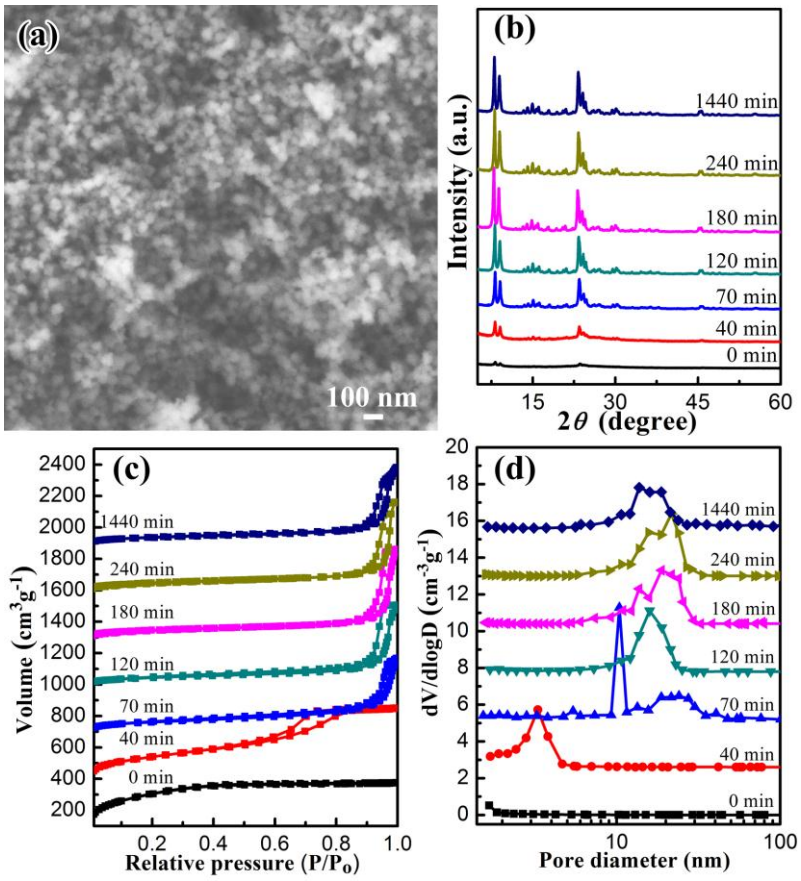

Fig. 7. Investigation on the crystallization process of NZS-60. (a) SEM image of the product crystallized at 180 ^{o}C for 180 min, (b) XRD patterns, (c) Nitrogen adsorption/desorption isotherms, and (d) BJH pore size distribution calculated from the adsorption branch of the isotherm for the samples crystallized at various crystallization time.

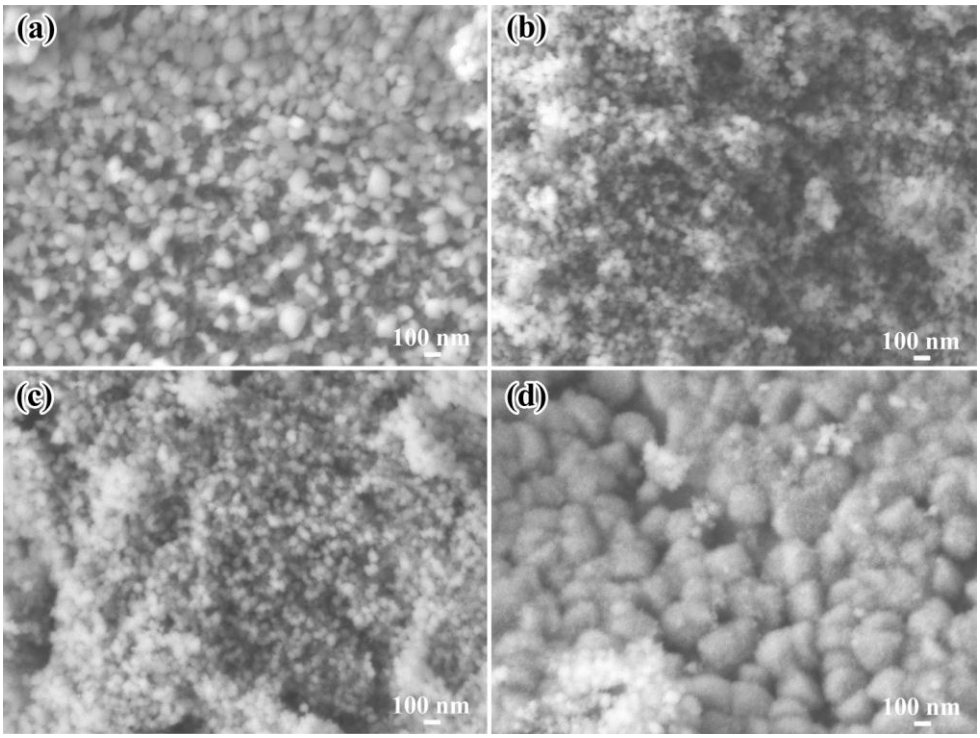

Fig. 8. SEM images of the NZS-60 prepared with an NH_4NO_3/SiO_2 molar ratio of (a) 0, (b) 0.017, (c) 0.034, and (d) 0.067, indicating that a trace amount of NH_4NO_3 addition to precursor gel markedly reduce the particle sizes of the NZS-60.

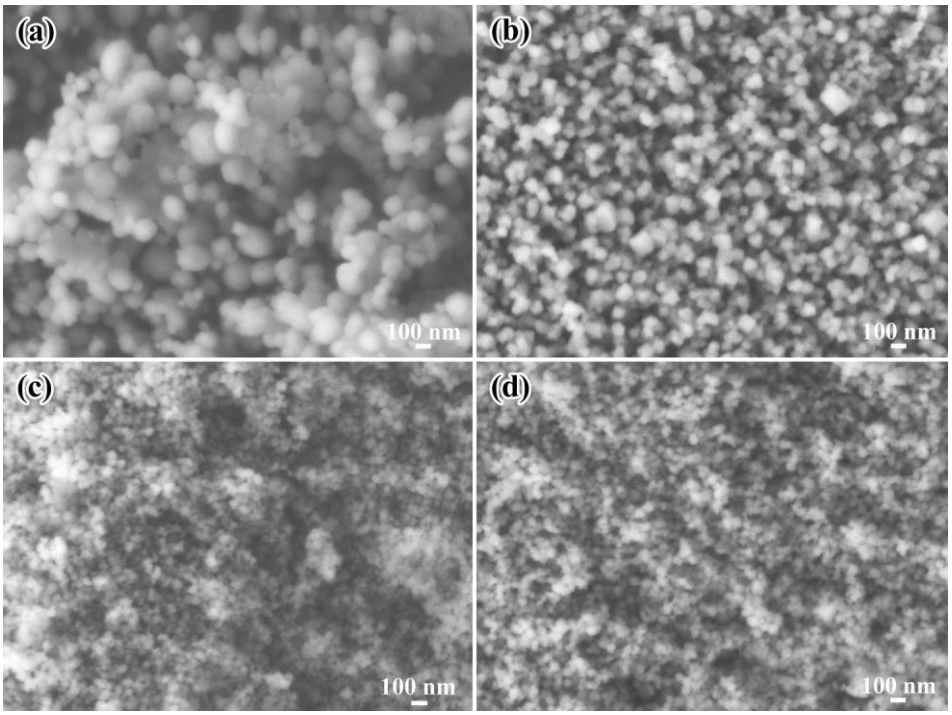

Fig. 9. SEM images of the NZS-60 prepared with an aging time of (a) 0 h, (b) 36 h, (c) 72 h, and (d) 144h, indicating that the particle size of NZS-60 is decreased with an increase in the pre-aging time.

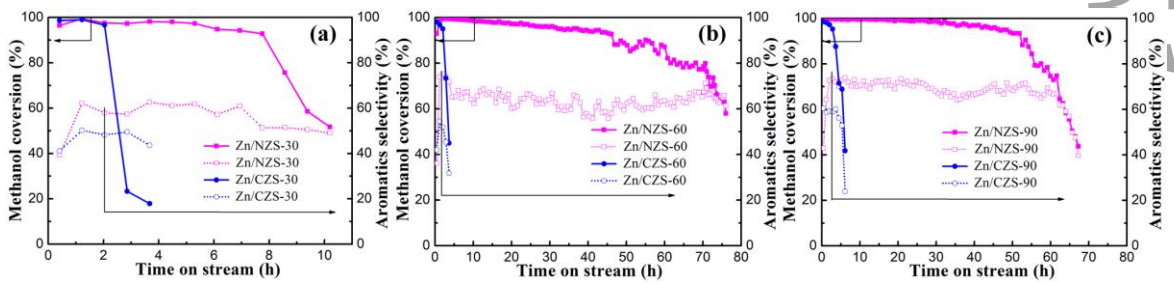

Fig. 10. Methanol conversions and overall aromatics selectivity with various Zn/ZSM-5 samples as a function of time-on-stream (reaction temperature: 475 ^{o}C; reaction pressure: atmospheric pressure, WHSV: 0.75 h^{-1}).

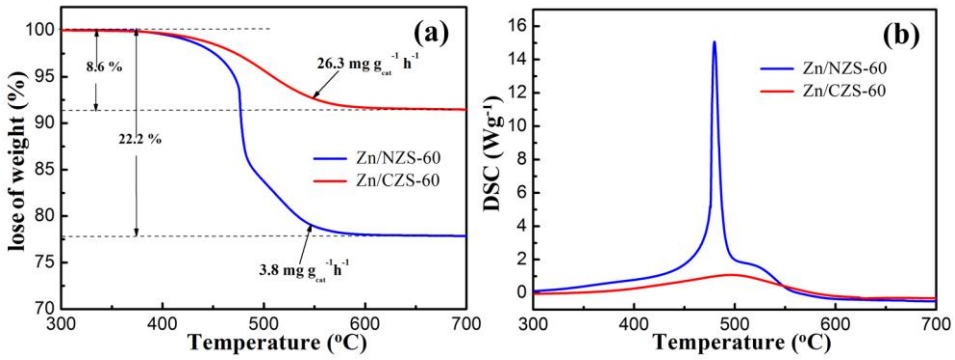

Fig. 11. (a) TG and (b) DSC profiles of the spent Zn/CZS-60 and Zn/NZS-60. Oxidation gas :20%O_2/N_2, heating rate 10 ^{o}C min^{-1}.

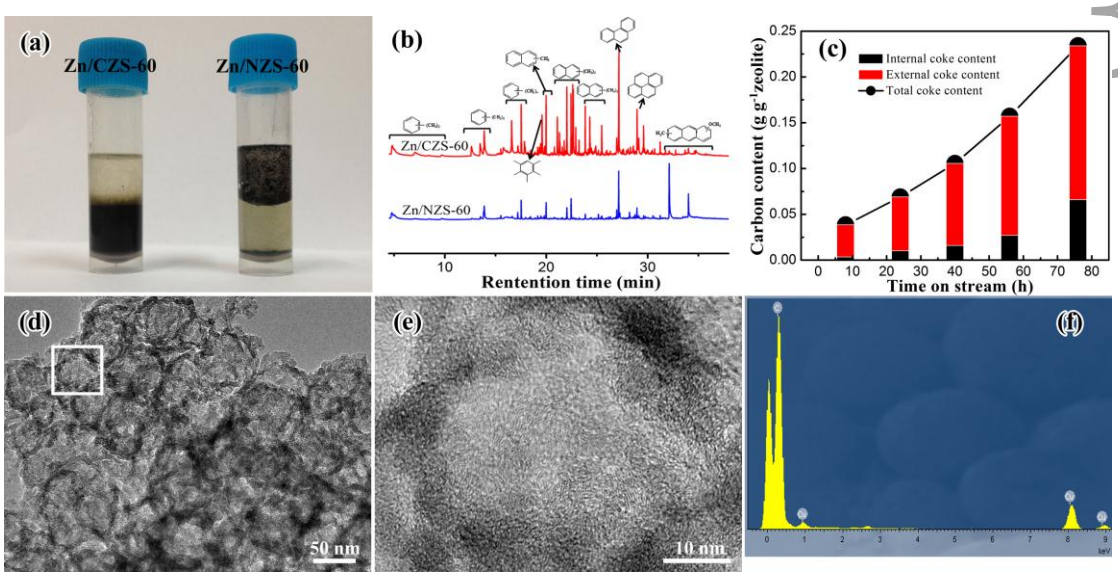

Fig. 12. (a) Photographs of the spent catalysts after being dissolved in 15% HF and extracted by CCl_4. (b) GC-MS chromatograms of the organic species in spent catalysts extracted by CH_2Cl_2. (c) Coke formation over Zn/NZS-60 with various time-on-stream during MTA reaction. (d) and (e) TEM images of the graphite carbon depositing on the outer surface of Zn/NZS-60 after the inner Zn/NZS-60 being dissolved by 15% HF solution. (f) The corresponding EDX spectrum of the graphite carbon.

Graphical Abstract

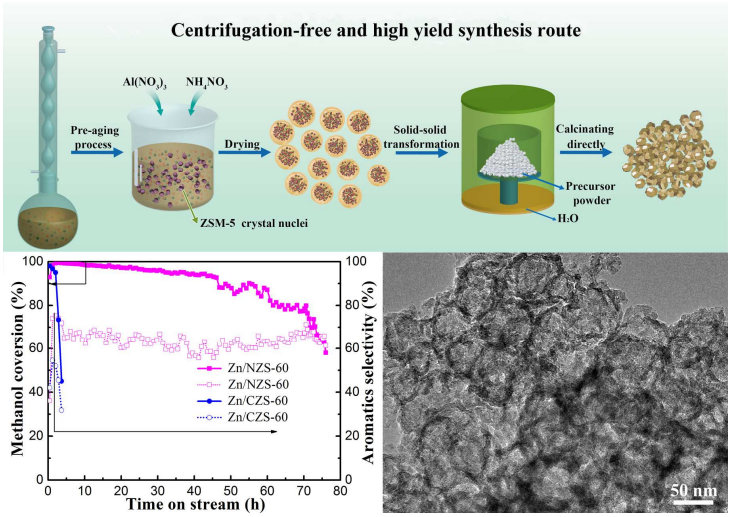

Nanosized H-ZSM-5 with excellent structural properties is first synthesised using a centrifugation-free and high yield synthesis route. The nanosized ZSM-5 shows superior catalytic stability and higher 1, 2, 4-trimethylbenzene selectivity when used in the catalytic conversion of methanol to aromatics.